PCCP

Cite this: *Phys. Chem. Chem. Phys.*, 2011, **13**, 6029–6035

www.rsc.org/pccp

**PAPER**

# Low-temperature formation of cubic β-$PbF_2$: precursor-based synthesis and first-principles phase stability study†

**Christoph Erk,[a] Lukas Hammerschmidt,[b] Dirk Andrae,[b] Beate Paulus*[b] and Sabine Schlecht*[a]**

***Received 8th September 2010, Accepted 27th January 2011***
**DOI: 10.1039/c0cp01758b**



A precursor-based approach to the cubic β-phase of $PbF_2$ was developed and allowed the preparation of this high-temperature phase well below the temperature for transition from the orthorhombic α- to the cubic β-phase. The formation of β-$PbF_2$ from the molecular precursors $Pb[Se(C_6H_2(CF_3)_3)]_2$ and $Pb(C_6H_2(CF_3)_3)_2$ is facilitated by the presence of several short Pb···F contacts in these molecules. The cubic form of $PbF_2$ was obtained as macroscopic crystals as well as nanoparticulate powder. Its formation at relatively low temperature suggested a theoretical re-investigation of the phase stabilities of the two polymorphs. The theoretical results from the Kohn–Sham density functional theory indicate that the energy content for the β-phase is slightly lower than the one for the α-phase, by 0.5–1.7 kJ $mol^{-1}$ depending on the density functional used (zero-point vibrational energy correction included).

## 1 Introduction

Two polymorphs of lead(II) fluoride are known to exist under ambient conditions, the orthorhombic α-$PbF_2$[1] and the cubic β-$PbF_2$,[2] see Fig. 1 for their crystal structures. Both forms have highly interesting physico-chemical properties: the α-polymorph is a promising candidate material for scintillation detectors in high energy physics experiments, due to its luminescence properties,[3] whereas the β-polymorph becomes a superionic conductor at the relatively low transition temperature of $T_c \approx 710$ K.[4–6] In the conducting high-temperature phase, sometimes considered as a third polymorph (denoted β′or β*),[6,7] the sublattice of the carriers of conductivity, the fluoride ions, is partially disordered due to an increase of Frenkel defects.[8–10]

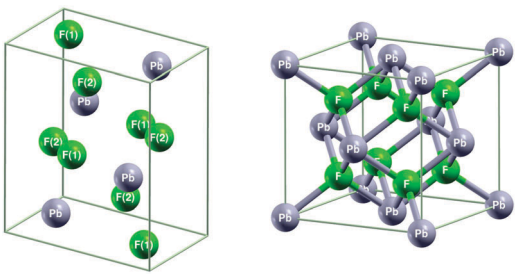


**Fig. 1** Crystal structures of orthorhombic cotunnite-type α-$PbF_2$ (left) and cubic fluorite-type β-$PbF_2$ (right); both cells shown contain $Z = 4$ formula units.

The cubic β-phase crystallizes from the melt ($T_m \approx 1103$ K) under ambient pressure. A pressure-induced irreversible phase transition to the orthorhombic α-phase takes place at room temperature and a pressure of about 0.5 GPa.[4–6,11] At about 610 K and under ambient pressure the reverse transition (α → β) occurs. It is still unclear which of the two polymorphs is the thermodynamically stable one under ambient conditions. Electrochemical experiments with a $Pb/\alpha\text{-}PbF_2//KF_{(aq)}//\beta\text{-}PbF_2/Pb$ cell[12] indicated the β-phase to be more stable than the α-phase, but this conclusion has been questioned later on the basis of data from high-pressure differential thermal analysis[13] and of pressure- and temperature-dependent elastic constants data for the cubic β-phase.[7] Additional experimental evidence for the β-phase as the thermodynamically stable polymorph was provided by precipitation experiments forming $PbF_2$ from aqueous solutions of lead(II) nitrate, $Pb(NO_3)_2$, and ammonium fluoride, $NH_4F$.[14] In this early work it was found that β-$PbF_2$ was formed when the precipitation was slow whereas a fast precipitation, which is rather prone to the formation of a metastable product, yielded α-$PbF_2$. Similarly, only the α-phase was formed in the fast precipitation observed upon addition of lead(II) oxide to concentrated hydrofluoric

[a] *Institut für Anorganische und Analytische Chemie, Justus-Liebig-Universität Giessen, Heinrich-Buff-Ring 58, D-35392 Giessen, Germany. E-mail: sabine.schlecht@anorg.chemie.uni-giessen.de*
[b] *Physikalische und Theoretische Chemie, Institut für Chemie und Biochemie, Freie Universität Berlin, Takustrasse 3, D-14195 Berlin, Germany. E-mail: beate@chemie.fu-berlin.de*

† Electronic supplementary information (ESI) available: Optimized geometric parameters and associated energetic data calculated for the equilibrium crystal structures of both polymorphs and for the isolated monomer; complete sets of calculated single-crystal elastic constants. See DOI: 10.1039/c0cp01758b

acid.[1] Further theoretical support for this energetic relation between the two polymorphs came from a recent first-principles study,[15] using pseudopotentials with plane waves as a basis set, which found the β-phase to be more stable than the α-phase, by 2–7 kJ $mol^{-1}$, depending on pseudopotential and exchange–correlation functional used. Yet another recent first-principles study[16] of three phases of $PbF_2$ (cubic, orthorhombic and hexagonal) used effective core potentials with linear combinations of Gauss-type functions as a basis set, but focused on the electronic band structures and densities of states of these three phases. Only the geometric crystal structure parameter of the cubic β-phase was fully optimized, but those for the other two phases were taken from earlier work[17] done with the *ab initio* perturbed ion method (*ai*PI, a Hartree–Fock method for the solid using a localized Fock space) augmented with a correlation energy estimate from density functional theory (DFT-*ai*PI).

The experimental part of our work presents a new precursor-based synthetic route to cubic β-$PbF_2$ where the product is formed well below the phase-transition temperature of 610 K. This experimental result asked for further theoretical studies of the two polymorphs of lead(II) fluoride. The primary purpose of these latter investigations was the comparative study of the relative energetics of the two phases. In contrast to previous work available in the literature our first-principles study is not only based on a single density functional, but also applies the full range of functionals available today, from the simple local density approximation (LDA) to the technically more demanding hybrid functionals that include the Hartree–Fock exchange, in order to achieve a consistent and reliable result. For each of the two polymorphs, the geometric crystal structure has been fully optimized. In addition, complete sets of single-crystal elastic constants have been calculated.

## 2 Experimental and computational details

### 2.1 Crystal structures of the two $PbF_2$ polymorphs

For the discussions to follow a detailed description of the crystal structures of the two polymorphs of $PbF_2$ is useful.

α-$PbF_2$ crystallizes in the orthorhombic cotunnite-type structure (space group *Pnma*, no. 62, $a = 644.0$ pm, $b = 389.9$ pm, $c = 765.1$ pm, $Z = 4$),[1] see Fig. 1. All atoms occupy Wyckoff 4(c) sites at $\pm(x, \frac{1}{4}, z)$ and $\pm(\frac{1}{2} - x, \frac{3}{4}, \frac{1}{2} + z)$. Hence, this structure has a total of nine degrees of freedom. Each $Pb^{2+}$ ion is surrounded by nine $F^-$ ions located at the corners of a distorted tricapped trigonal prism, with Pb–F distances ranging from 241 pm to 303 pm. One half of the $F^-$ ions in the unit cell, labelled F(1) in Fig. 1, is coordinated by four $Pb^{2+}$ ions arranged in a slightly distorted tetrahedron. The other half, labelled F(2), is coordinated by five $Pb^{2+}$ ions arranged in a distorted quadratic pyramid, with three closer-lying cations, but in this case two other $F^-$ ions already lie slightly closer (296 pm) than the most distant cations.

The other polymorph, β-$PbF_2$, crystallizes in the cubic fluorite-type structure (space group $Fm\bar{3}m$, no. 225, $a = 594.6$ pm, $Z = 4$),[2] see Fig. 1. The $Pb^{2+}$ ions occupy Wyckoff 4(a) sites at (0,0,0) + fc,‡ whereas the $F^-$ ions are in Wyckoff 8(c) positions at $(\frac{1}{4}, \frac{1}{4}, \frac{1}{4})$ + fc and at $(\frac{1}{4}, \frac{1}{4}, \frac{3}{4})$ + fc. The cell parameter is the only degree of freedom of this structure. The $Pb^{2+}$ ions are coordinated by eight $F^-$ ions, which are themselves placed at the centres of tetrahedra formed by four $Pb^{2+}$ ions. The nearest-neighbour Pb–F distance in the cubic polymorph is $\frac{1}{4}\sqrt{3}\,a = 257$ pm.

### 2.2 Experimental details

Lead(II) 2,4,6-tris(trifluoromethyl)selenophenolate, $Pb[Se(C_6H_2(CF_3)_3)]_2$, and bis(2,4,6-tris(trifluoromethyl)phenyl) lead(II), $Pb(C_6H_2(CF_3)_3)_2$, were synthesized according to methods described in the literature.[18,19] Hexamethyldisilazane, 1,3,5-tris(trifluoromethyl)benzene, *n*-butyl lithium solution (1.6 M in hexane) and tetrafluoroboric acid diethyl ether complex were purchased from Aldrich and used as received. Lead(II) hexamethyldisilyl amide was synthesized according to the method described by Gynane *et al.*[20] All solvents were dried and distilled prior to use, and all synthetic operations were conducted in an argon atmosphere, unless stated otherwise. Thermal decomposition experiments of lead(II) 2,4,6-tris-(trifluoromethyl)selenophenolate and bis(2,4,6-tris(trifluoromethyl)phenyl) lead(II) were carried out in a Schlenk glass tube. A small amount of the precursor was placed onto a glass slide inside the tube. The Schlenk tube was placed in a furnace (HTM Reetz Losa tube furnace with a Eurotherm 2132 PID temperature control unit, max. temperature 600 °C). The temperature was raised by 10 K per min from room temperature to the desired final temperature, and held there for the desired length of time for thermolysis. The glass tube was then removed from the oven and allowed to cool down to room temperature.

X-Ray powder diffraction patterns were recorded with a Stoe Stadi P transmission powder diffractometer and a Philips PW 1700 series reflection powder diffractometer, both using Cu-Kα radiation.

Transmission electron microscopy was performed using a Jeol JEM 1010 and a Philips CM12 transmission electron microscope, both operated at 100 kV ($LaB_6$ cathode). For sample preparation the product powders were carefully dispersed onto carbon coated copper grids.

### 2.3 Computational details

First-principles calculations based on the Kohn–Sham density functional theory (KS-DFT) were carried out, using five different density functionals. These comprised a functional based on the local density approximation (LDA) and denoted here as SVWN,[21–23] two functionals based on the generalized gradient approximation (GGA) denoted as PBE[24] and PW91[25] and, finally, two hybrid functionals, B3LYP[26,27] and B3PW,[25,26] differing only in the correlation functional.

Periodic self-consistent field (SCF) calculations were performed with the CRYSTAL06 programme,[28] whereas the MOLPRO suite of programmes[29] was used for SCF calculations of the isolated monomer and for counterpoise-corrected[30]

‡ 'fc' denotes one of the face centering translations (0,0,0), $(0, \frac{1}{2}, \frac{1}{2})$, $(\frac{1}{2}, 0, \frac{1}{2})$, or $(\frac{1}{2}, \frac{1}{2}, 0)$

 

calculations of the ions. Gauss-type function basis sets (LC-GTO) were used, together with an energy-consistent scalar-relativistic effective core potential (ECP) simulating the chemically inactive [Kr] $4d^{10}$ $4f^{14}$ core of the Pb atom.[31] For the crystal calculations and for the counterpoise-corrected calculations of the ions a modified cc-pVDZ basis set for lead[32] and a 7-311G basis set for fluorine[33] were used. Basis sets for calculations of the isolated monomer were obtained from the crystal basis sets by adding one diffuse function in each symmetry (with parameter taken as half the smallest one present in the crystal basis). The monomer energies thus obtained compare very well with data from calculations using cc-pVDZ or cc-pVTZ basis sets.

The calculation of single-crystal elastic constants requires well converged crystal structures and energies. In all calculations an energy convergence threshold of at least $10^{-8}$ $E_h$ was imposed, and optimizations of crystal and monomer structures were carried on until an energy gradient threshold of $10^{-7}$ $E_h$ per pm was met ($E_h$ = 1 hartree is the atomic unit of energy[34]). In the crystal calculations the total number of $k$-space points in the irreducible Brillouin zone was 343 for the orthorhombic case and 72 for the cubic case, respectively.

The elastic constants $C_{ij}$ (in Voigt's notation) were determined from their definition that relates them to mixed second derivatives of the crystal cell energy $E$ with respect to components $\varepsilon_i$, $\varepsilon_j$ of the dimensionless strain tensor.[35,36] For each elastic constant, ten slightly distorted crystal structures were considered and fully optimized with respect to their internal degrees of freedom. The resulting energies $E(\delta)$ were fitted to a fourth-order polynomial (the scalar $\delta$ parametrizes the strain tensor for the particular deformation under consideration, and was chosen such that $|\delta| \leq 0.01$). The second derivative $E''(0)$ is related to the desired elastic constant (or, in general, to a linear combination of such constants). Finally, for each polymorph, the energies already used for the determination of the bulk modulus $B_0$ were used again for a non-linear least squares fit to the Murnaghan equation of state,[37,38] and thereby gave another estimate for the bulk modulus $B_0$ and its pressure derivative $B_0'$. The pressure $P_{\beta\rightarrow\alpha}$ for phase transition from the cubic to the orthorhombic polymorph was estimated from the common tangent[39] to the two equations of state.

## 3 Results and discussion

### 3.1. Experimental results

Fluorinated organometallic compounds are known to be useful molecular precursor systems for the thermolytic preparation of binary fluorides with interesting material properties.[40] Thus, a molecular precursor approach starting from molecular lead(II) compounds with fluorinated organic substituents was also attempted for lead fluoride, $PbF_2$. Here it had to be taken into account that such lead(II) compounds containing fluorinated organic moieties are rare and not easy to prepare because of their electron-poor and coordinatively unsaturated nature. Among the well characterized and fairly stable candidates are the fluorinated

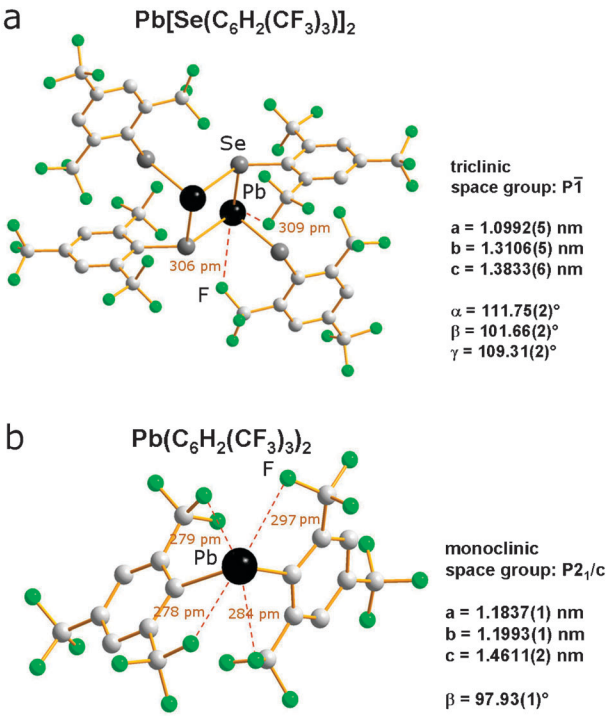


**Fig. 2** Molecular structures of (a) $Pb[Se(C_6H_2(CF_3)_3)]_2$ according to ref. 18, and of (b) $Pb(C_6H_2(CF_3)_3)_2$ according to ref. 19, with indication of some important short Pb–F distances in both cases.

mesityl derivatives $Pb[Se(C_6H_2(CF_3)_3)]_2$[18] (which forms a dimer) and $Pb(C_6H_2(CF_3)_3)_2$.[19]

In both compounds short Pb···F contacts are present. This leads to a weakening of the C–F bonds and a relative stabilisation of the Pb(II) centre in these molecules. The lead(II) 2,4,6-tris(trifluoromethyl)selenophenolate crystallizes as a dimer (Fig. 2a) and the shortest Pb···F distances are found as 306 pm and 309 pm. Two more short Pb···F interactions are found which are still well below the sum of van-der-Waals radii of Pb and F of 350 pm.[41] This binding situation leads to a low temperature formation of $PbF_2$ from the precursor starting at around 200 °C. At an even lower temperature of only 100 °C the formation of $PbF_2$ starts for the organolead compound $Pb(C_6H_2(CF_3)_3)_2$. In this case, the molecule crystallizes in monomeric form with only six valence electrons at the lead atom. The lead atom exhibits four very short Pb···F contacts between 278 pm and 297 pm to partly compensate for its electron deficiency (Fig. 2b). The shortest of these distances are already getting close to the Pb···F distance of 257 pm found in cubic β-$PbF_2$.[2] Therefore, the activation barrier for a thermolytic formation of the lead fluoride is low and only a small reconstruction of the atomic arrangement is necessary.

The thermolysis of the lead(II) 2,4,6-tris(trifluoromethyl)-selenophenolate was performed with a heating rate of 10 K $min^{-1}$ from room temperature to 400 °C. In Fig. 3 three different powder diffraction patterns of the products at 233 °C, 300 °C and 400 °C are depicted. The reflections can be assigned to cubic $PbF_2$ in the fluorite structure and to cubic PbSe crystallizing in the rocksalt structure. When the thermolysis is stopped at 233 °C the powder pattern shows

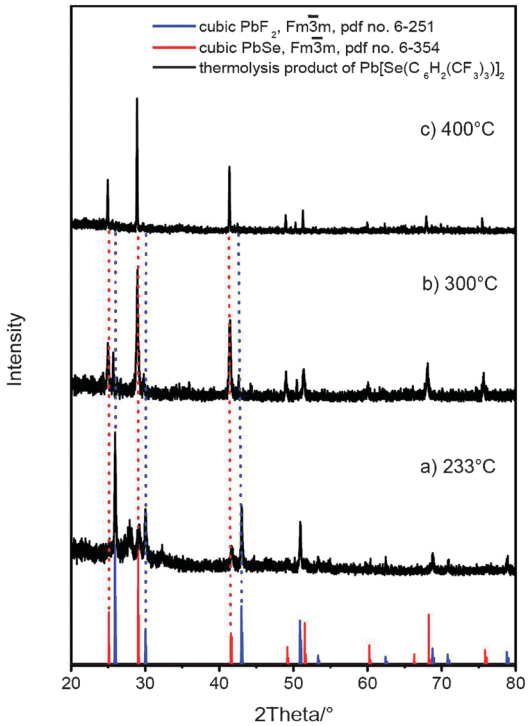


**Fig. 3** XRD patterns recorded from the thermolytic products of $Pb[Se(C_6H_2(CF_3)_3)]_2$ obtained at different temperatures [(a) 233 °C, (b) 300 °C and (c) 400 °C] and calculated XRD patterns of cubic $PbF_2$ (blue) and cubic PbSe (red).

intense reflections of β-$PbF_2$ and only the strongest reflections of PbSe appear with low intensity. The second powder pattern which was collected after thermolysis at 300 °C already exhibits much stronger reflections for PbSe with no increase of the intensities of the set of signals originating from $PbF_2$. When the thermolysis was continued to a final temperature of 400 °C only reflections of PbSe are detected and it can be concluded that the content of $PbF_2$ in the product obtained at this temperature is $<5\%$. These results make clear that the formation of β-$PbF_2$ from the fluorinated lead selenophenolate is the kinetically favoured initial low temperature process followed by the formation and crystallisation of PbSe at more elevated temperatures. The much higher diffraction intensity of PbSe makes the small amount of $PbF_2$ present in the final product disappear into the background. It is remarkable though, that the PbSe obtained from these thermolyses is a very fine black powder whereas the $PbF_2$ formed at an early stage of the decomposition forms much larger colourless crystals of 200–500 μm size. These differences in grain size are also reflected by the half widths of the two sets of reflections observed in the powder patterns (Fig. 3). Not only the grain formation of $PbF_2$ but also its grain growth do not seem to compete yet with a grain formation of PbSe at this early stage of the thermolysis.

The problem of competing thermolytic pathways leading to different products does not arise when $Pb(C_6H_2(CF_3)_3)_2$ is thermolyzed. As already said, this precursor has four very short Pb···F contacts and weakened C–F bonds. Therefore, it is not surprising that the formation of $PbF_2$ already starts at approximately 60 °C. The yellow crystals turn dark and first

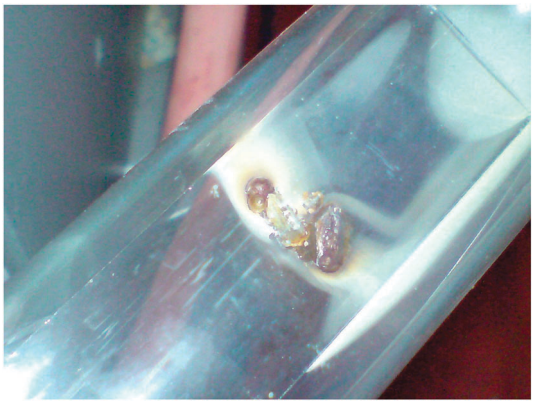

**Fig. 4** Thermolytic product $PbF_2$ obtained from $Pb(C_6H_2(CF_3)_3)_2$ at 155 °C.

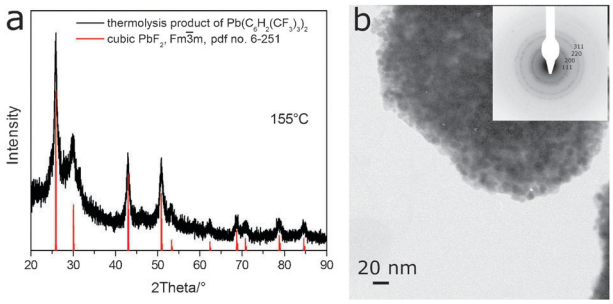


**Fig. 5** (a) XRD pattern recorded from the thermolytic product of $Pb(C_6H_2(CF_3)_3)_2$ obtained at 155 °C; (b) corresponding TEM image and SAED pattern (inset), indexed for cubic $PbF_2$.

signs of a decomposition become visible. At about 100 °C the formation of a fine white solid can be observed which becomes much more intense at 150 °C. The thermolytic product produced at 155 °C is shown in Fig. 4. The produced solid was characterized by powder diffraction and TEM investigation. Both methods clearly identified the product as crystalline $PbF_2$ in its β-form (Fig. 5). No formation of α-$PbF_2$ or elemental lead was observed. The reflections of β-$PbF_2$ in the diffractogramme are significantly broadened (Fig. 5a) and an estimate of the grain size derived from the Scherrer equation is ∼6 nm. The TEM micrographs of the sample are in good accordance with this value. They show large agglomerates of small individual particles of 8.7 ± 18 nm diameter (Fig. 5b). Their crystallinity is high as can be seen in the SAED pattern which can also be indexed for β-$PbF_2$ (Fig. 5b, inset).

A second thermolysis was performed where the precursor was heated to 250 °C and held at the temperature for one hour. Again, off-white $PbF_2$ was produced, but a black minor by-product was also observed. The $PbF_2$ obtained in this way was characterized by X-ray powder diffraction and transmission electron microscopy (Fig. 6). The diffractogramme as well as the SAED pattern show single-phase material with good crystallinity. The reflections are much less broadened, indicating a larger length of coherence and particle size. From the Scherrer equation a value of 23 nm can be obtained as a mean diameter. This is in fair agreement with the average

 

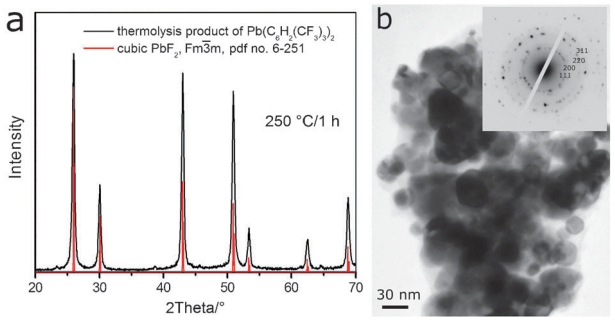


**Fig. 6** (a) XRD pattern recorded from the thermolytic product of $Pb(C_6H_2(CF_3)_3)_2$ obtained at 250 °C after 1 h; (b) corresponding TEM image and SAED pattern (inset), indexed for cubic $PbF_2$.

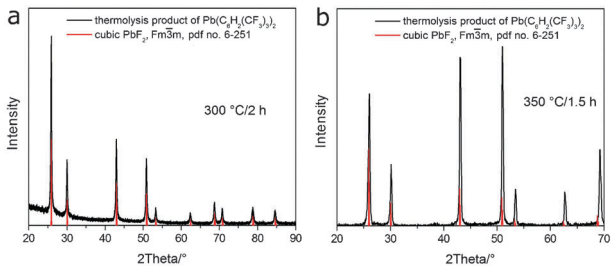


**Fig. 7** Powder diffraction patterns of the thermolysis products obtained from $Pb(C_6H_2(CF_3)_3)_2$ at 300 °C per 2 h (a) and at 350 °C per 1.5 h (b).

particle diameter of 30 ± 11 nm found in the TEM images (Fig. 6b). The grain size of the β-$PbF_2$ formed from $Pb(C_6H_2(CF_3)_3)_2$ at a temperature of 250 °C is very different and very much smaller than for the β-$PbF_2$ obtained from the selenolate $Pb[Se(C_6H_2(CF_3)_3)]_2$ at 233 °C. Apart from the faster grain formation associated with the shorter Pb···F contacts in the organolead compound this might also be due to a difference in volatility of the two precursors. In the case of $Pb(C_6H_2(CF_3)_3)_2$ a certain degree of evaporation and sublimation of the intact precursor molecules was observed and the formation of white $PbF_2$ from the gas phase could be found. This leads to a continuous formation of new grains instead of grain growth during the decomposition process. Further thermolytic experiments were conducted at 300 °C and at 350 °C with holding times of 2 h and 1.5 h, respectively. The solid produced in these thermolyses is brownish and much darker than the $PbF_2$ obtained at lower temperature, indicating a higher degree of carbonization at more elevated temperatures. The products were characterized by powder diffraction patterns (Fig. 7). The X-ray diffraction data show cubic single-phase $PbF_2$ and no additional reflections of any crystalline by-products. The reflections are not broadened and the particles obtained at 300 °C or 350 °C have diameters >200 nm. The differences in reflection intensities observed in the powder patterns depicted in Fig. 7a and b are caused by the use of different apparatus, not by different morphologies of the solid products.

### 3.2 Theoretical results

Essential theoretical results are collected in Table 1, together with other theoretical and experimental data for comparison. Additional detailed theoretical results can be found as ESI.†

Comparison of the calculated crystal unit cell structures with experimental and other theoretical data (equilibrium volume, bulk modulus and its pressure derivative in Table 1, other data in ESI†) shows that both polymorphs are reasonably well described with all functionals except SVWN (LDA). As expected, since well known for this[15] and many other cases, this latter functional yields crystal structures that are too compact and have a much too large bulk modulus. The GGA and hybrid functionals, on the other hand, yield

**Table 1** Equilibrium crystal cell parameters and parameters for the Murnaghan equation of state[37,38] for both polymorphs of lead(II) fluoride, $PbF_2$, and derived phase-stability data (see also Fig. 8), other theoretical and experimental data for comparison

| | α-$PbF_2$ (orthorhombic) | | | | β-$PbF_2$ (cubic) | | | | | | |
|---|---|---|---|---|---|---|---|---|---|---|---|
| | $V_{0,\alpha}{}^a/10^{-3}$ nm$^3$ | $E_{b,\alpha}{}^b$/eV | $B_{0,\alpha}$/GPa | $B'_{0,\alpha}$ | $V_{0,\beta}{}^a/10^{-3}$nm$^3$ | $E_{b,\beta}{}^b$/eV | $B_{0,\beta}$/GPa | $B'_{0,\beta}$ | $\Delta E_0{}^c$/kJ mol$^{-1}$ | $-\Delta V_0{}^d/10^{-3}$nm$^3$ | $P_{\beta\rightarrow\alpha}{}^e$/GPa |
| This work | | | | | | | | | | | |
| SVWN | 174.92 | −2.38 | 80.1 | 7.47 | 193.06 | −2.45 | 96.3 | 4.65 | −6.04 | 18.20 | — |
| PBE | 196.22 | −1.55 | 50.9 | 5.09 | 211.11 | −1.53 | 74.5 | 3.00 | 1.85 | 14.86 | 0.80 |
| PW91 | 194.63 | −1.57 | 51.8 | 5.26 | 209.80 | −1.55 | 76.0 | 4.81 | 2.17 | 15.16 | 0.92 |
| B3LYP | 199.07 | −1.50 | 49.8 | 8.37 | 212.61 | −1.47 | 75.0 | 8.13 | 3.09 | 13.45 | 1.44 |
| B3PW | 193.97 | −1.34 | 49.5 | 9.01 | 208.28 | −1.31 | 76.7 | 8.72 | 3.07 | 14.35 | 1.36 |
| Other calculations | | | | | | | | | | | |
| HF[f] | — | — | — | — | 204.34 | — | 87.5 | 4.47 | — | — | — |
| DFT-*ai*PI[g] | 196.61 | — | 57.9 | 4.98 | 214.38 | — | 56.0 | 4.90 | — | 17.77 | 1.98 |
| B3LYP[h] | — | — | — | — | 213.85 | — | 60.4 | 4.84 | — | — | — |
| LDA[i] | 181.91 | — | — | — | 198.36 | — | — | — | — | 16.45 | — |
| GGA[i] | 205.58 | — | 63.2 | — | 219.15 | — | 69.7 | — | — | 13.57 | — |
| Experiment[j] | 192.11 | (−2.50) | 56.0 | 7.9 | 210.25 | (−2.50) | 69.5 | 7.5 | — | 18.14 | 0.50 |

[a] Volumes refer to unit cells containing $Z = 4$ formula units (as shown in Fig. 1), see also Table S1 in ESI.[1] [b] Total energy difference for $PbF_2$(g) → $PbF_2$(α or β), see also Table S2 in ESI.† [c] Energy difference $\Delta E_0 = E_{0,\alpha} - E_{0,\beta}$ per mole of formula units, see also Table S2 in ESI.† [d] Volume difference $\Delta V_0 = V_{0,\alpha} - V_{0,\beta} < 0$. [e] Transition pressure (obtained from the common tangent method in this work). [f] Ref. 42 (periodic HF, effective core potential, LC-GTO). [g] Ref. 17 (*ab initio* perturbed ion HF approach augmented by DFT for correlation energy, see Table S1 in ESI† for further details). [h] Ref. 16 (periodic DFT, effective core potential, LC-GTO). [i] Ref. 15 (periodic DFT, pseudopotential, plane waves, see Table S3 in ESI† for further details). [j] Volumes from ref. 1 and 2; binding energy estimated from $\Delta_f H°$(298.15 K) from ref. 43; bulk moduli (extrapolated to 0 K) and their pressure derivatives from ref. 44 and 15 for α-$PbF_2$, and from ref. 7 for β-$PbF_2$.

equilibrium volumes deviating from the respective experimental values, determined under ambient conditions, by at most 3.6% (orthorhombic phase) and 1.2% (cubic phase). The bulk modulus, which is obtained always too large with these same functionals, deviates by at most 10% from experiment. As in experiment, the bulk modulus calculated for the cubic phase is always found larger than the one for the orthorhombic phase. The larger relative scatter in our data for the pressure derivative of the bulk modulus, with respect to both experiment and other calculations, reflects the higher sensitivity of this quantity with respect to details in the applied methods. Anyway, we find a very reasonable overall agreement between our data characterizing the crystal unit cell, calculated with hybrid functionals, and the corresponding experimental values.

Lattice energies $E_{lat}$, *i.e.*, energies associated with the reactions $Pb^{2+}(g) + 2\ F^{-}(g) \rightarrow PbF_2(\alpha \text{ or } \beta)$, cannot be determined with confidence with available standard KS-DFT (because *all* functionals used here describe the $F^-$ ion as an autoionizing system, with *positive* highest orbital energy). Therefore, the binding energy $E_b$ for the reactions $PbF_2(g) \rightarrow PbF_2(\alpha \text{ or } \beta)$ was considered, and calculated as difference between the energy per formula unit in the solid and the counterpoise-corrected monomer energy. Thermodynamic data for this reaction are available,[43] though with considerable uncertainty as to the character of the crystalline phase involved in the experiments (carried out at room temperature, not at 0 K). Nevertheless, if we compare the calculated binding energies with the experimental value, all functionals, except the LDA funtional SVWN, underestimate it by about 40%. Surprisingly, the LDA functional yields a result in much closer agreement with experiment, most probably due to error cancellation: binding is overestimated, compared to the results obtained with the other functionals, due to the too small lattice parameters. The underestimation in binding energy, found with the GGA and hybrid functionals, can be due to the improper description of correlation of the closed 5d shell of Pb. As observed, *e.g.*, in solid mercury, this can contribute significantly to the binding (in the case of solid mercury about 50%).[45] A detailed analysis of correlation effects in $PbF_2$ would only be possible within a wavefunction-based correlation treatment, *e.g.*, with the method of increments,[46] which is beyond the scope of this work.

Total energy differences between the two polymorphs were found to be very small, and favour the cubic β-polymorph over the orthorhombic α-polymorph in all cases, except, again, for the LDA functional SVWN. Calculations using GGA or hybrid functionals showed β-$PbF_2$ to be 1.8–3.1 kJ $mol^{-1}$ more stable than α-$PbF_2$. This compares well with the 2–7 kJ $mol^{-1}$ found as uncorrected athermal energy difference in favour of the β-polymorph in a recent first-principles study.[15] Addition of the zero-point vibrational energy difference, estimated from the Debye theory (see ESI†), shifts our range of calculated total energy differences to 0.5–1.7 kJ $mol^{-1}$, but does not invert the energetic order of the two polymorphs. Additional vibrational energy has been estimated, from lattice dynamics within the harmonic approximation, to be very similar for the two polymorphs.[15]

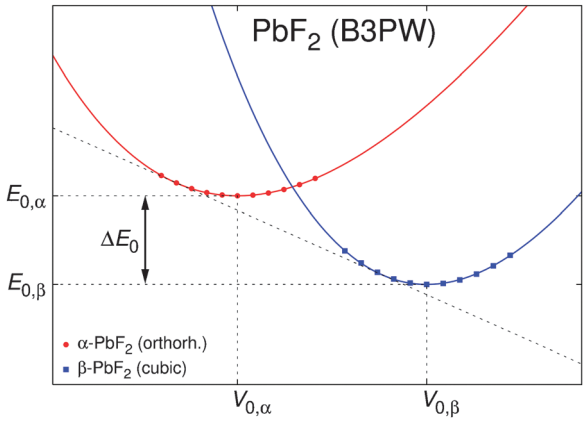


**Fig. 8** Total energy $E$ as a function of crystal cell volume $V$ for both polymorphs of lead(II) fluoride, $PbF_2$: calculated data (circles and squares), curves representing Murnaghan's equation of state[37,38] fitted to them (see also Table 1), and their common tangent.

The elastic constants $C_{ij}$ were obtained with good accuracy, as can be seen from those cases where comparison to available experimental values is possible (see ESI†). The $E(V)$ data used for the determination of the bulk modulus were also used in a non-linear least squares fit to the Murnaghan equation of state.[37,38] The alternative bulk modulus obtained in this way (see Table 1) was always found to be in very close agreement with the one determined from the elastic constants (see Table S3 of ESI†). The common tangent method[39] was applied to obtain the transition pressure $P_{\beta\rightarrow\alpha}$ from the two curves (Fig. 8 schematically shows the situation for the B3PW data). The LDA results for $E(V)$ prove unphysical here, since they lead to a negative transition pressure. The transition pressures, found from GGA or hybrid functional data (all at compressions of about $x = V/V_0 \approx 0.98$), are in reasonable agreement with the experiment, given the approximations, and hence uncertainty, in the calculations (referring to an athermal ideal crystal at 0 K, whereas the experimental value corresponds to a real crystals at room temperature, performing lattice vibrations and having defects).

More details on geometric parameters, energetic data and single-crystal elastic constants for the two polymorphs, with connection to further data and background information,[47–50] can be found as ESI.†

## 4 Conclusions

The thermolyses of the molecular precursors $Pb[Se(C_6H_2(CF_3)_3)]_2$ and $Pb(C_6H_2(CF_3)_3)_2$ lead to the formation of cubic β-$PbF_2$ at relatively low temperatures. The decomposition of $Pb(C_6H_2(CF_3)_3)_2$ produces nanoparticles of β-$PbF_2$ the size of which can be controlled by the decomposition temperature. The thermolysis of $Pb[Se(C_6H_2(CF_3)_3)]_2$ leads to the formation of microcrystalline β-$PbF_2$ at an early stage of the degradation process. Especially the latter phenomenon suggests that β-$PbF_2$ might be the thermodynamically stable polymorph and not only the kinetically stabilized product under the conditions of its formation.

The crystal structures of the two polymorphs of lead(II) fluoride, α-$PbF_2$ (orthorhombic) and β-$PbF_2$ (cubic), were

 

found to be well represented by KS-DFT calculations, using the GGA and hybrid functionals applied in this study. Reasonable results for the monomer binding energies, *i.e.*, the total energy differences related to the reactions $PbF_2(g) \rightarrow PbF_2(\alpha \text{ or } \beta)$, were obtained. The total energy difference between the two polymorphs at 0 K was found to be very small, with the β-phase always being lower in energy than the α-phase, except in the case of the LDA functional SVWN. Our uncorrected athermal results are in the range 1.8–3.1 kJ $mol^{-1}$, and are shifted to 0.5–1.7 kJ $mol^{-1}$ upon inclusion of zero-point vibrational energy. Full sets of single-crystal elastic constants have been calculated for both polymorphs, and found to be in good agreement with experiment (exptl. data are available almost exclusively for the β-phase). From Murnaghan's equations of state, fitted to $E(V)$ data for both polymorphs, the pressure for the transition from the cubic β-phase to the orthorhombic α-phase was estimated and found to be in reasonable agreement with the experimental value.



## Acknowledgements

We gratefully acknowledge financial support received from the Fonds der Chemischen Industrie (Kekulé Fellowship to C. E.) and from the Deutsche Forschungsgemeinschaft (Priority Programmes 1165 "Nanowires and Nanotubes: From Controlled Synthesis to Functions" and 1178 "Experimental Charge Density as the Key to Understand Chemical Interactions"). We also like to thank the anonymous referees for their helpful comments.

## References

1 P. Boldrini and B. O. Loopstra, *Acta Crystallogr.*, 1967, **22**, 744–745.
2 S. Hull, P. Berastegui, S. G. Eriksson and N. J. G. Gardner, *J. Phys.: Condens. Matter*, 1998, **10**, 8429–8446.
3 D. L. Alov and S. I. Rybchenko, *J. Phys.: Condens. Matter*, 1995, **7**, 1475–1482.
4 G. A. Samara, *Phys. Rev. B: Solid State*, 1976, **13**, 4529–4544.
5 J. Oberschmidt and D. Lazarus, *Phys. Rev. B: Condens. Matter*, 1980, **21**, 2952–2961.
6 S. Hull and D. A. Keen, *Phys. Rev. B: Condens. Matter*, 1998, **58**, 14837–14844.
7 J. C. Jamieson, M. H. Manghnani, T. Matsui and L. C. Ming, *J. Geophys. Res., [Solid Earth Planets]*, 1986, **91**, 4643–4649.
8 K. Koto, H. Schulz and R. A. Huggins, *Solid State Ionics*, 1980, **1**, 355–365.
9 M. T. Hutchings, K. Clausen, M. H. Dickens, W. Hayes, J. K. Kjems, P. G. Schnabel and C. Smith, *J. Phys. C: Solid State Phys.*, 1984, **17**, 3903–3940.
10 J. P. Goff, W. Hayes, S. Hull and M. T. Hutchings, *J. Phys.: Condens. Matter*, 1991, **3**, 3677–3687.
11 E. D. D. Schmidt and K. Vedam, *J. Phys. Chem. Solids*, 1966, **27**, 1563–1566.
12 J. H. Kennedy, R. Miles and J. Hunter, *J. Electrochem. Soc.*, 1973, **120**, 1441–1446.
13 W. Klement, Jr. and L. H. Cohen, *J. Electrochem. Soc.*, 1979, **126**, 1403–1405.
14 Ya. Sauka, *Zh. Obshch. Khim.*, 1949, **19**, 1453–1458 (*Russ. J. Gen. Chem.*, 1949, **19**, 1453–1457).
15 A. Dubinin, B. Winkler, K. Knorr and V. Milman, *Eur. Phys. J. B*, 2004, **39**, 27–33.
16 H. Jiang, R. Orlando, M. A. Blanco and R. Pandey, *J. Phys.: Condens. Matter*, 2004, **16**, 3081–3088.
17 A. Costales, M. A. Blanco, R. Pandey and J. M. Recio, *Phys. Rev. B: Condens. Matter*, 2000, **61**, 11359–11362.
18 D. Labahn, F. M. Bohnen, R. Herbst-Irmer, E. Pohl, D. Stalke and H. W. Roesky, *Z. Anorg. Allg. Chem.*, 1994, **620**, 41–47.
19 S. Brooker, J. K. Buijink and F. T. Edelmann, *Organometallics*, 1991, **10**, 25–26.
20 M. J. S. Gynane, D. H. Harris, M. F. Lappert, P. P. Power, P. Rivière and M. Rivière-Baudet, *J. Chem. Soc., Dalton Trans.*, 1977, 2004–2009.
21 P. A. M. Dirac, *Proc. Cambridge Philos. Soc.*, 1930, **26**, 376–385.
22 J. C. Slater, *Phys. Rev.*, 1951, **81**, 385–390.
23 S. H. Vosko, L. Wilk and M. Nusair, *Can. J. Phys.*, 1980, **58**, 1200–1211.
24 J. P. Perdew, K. Burke and M. Ernzerhof, *Phys. Rev. Lett.*, 1996, **77**, 3865–3868.
25 J. P. Perdew and Y. Wang, *Phys. Rev. B: Condens. Matter*, 1992, **45**, 13244–13249.
26 A. D. Becke, *J. Chem. Phys.*, 1993, **98**, 5648–5652.
27 C. Lee, W. Yang and R. G. Parr, *Phys. Rev. B: Condens. Matter*, 1988, **37**, 785–789.
28 R. Dovesi, V. R. Saunders, C. Roetti, R. Orlando, C. M. Zicovich-Wilson, F. Pascale, B. Civalleri, K. Doll, N. M. Harrison, I. J. Bush, Ph. D'Arco and M. Llunell, *CRYSTAL06 User's Manual*, University of Torino, Torino, Italy, 2006, see http://www.crystal.unito.it/.
29 MOLPRO, a package of *ab initio* programs written by H.-J. Werner, P. J. Knowles, R. Lindh, F. R. Manby, M. Schütz, and others, see http://www.molpro.net/.
30 S. F. Boys and F. Bernardi, *Mol. Phys.*, 1970, **19**, 553–566.
31 B. Metz, H. Stoll and M. Dolg, *J. Chem. Phys.*, 2000, **113**, 2563–2569.
32 K. A. Peterson, *J. Chem. Phys.*, 2003, **119**, 11099–11112.
33 R. Nada, C. R. A. Catlow, C. Pisani and R. Orlando, *Modell. Simul. Mater. Sci. Eng.*, 1993, **1**, 165–187.
34 P. J. Mohr, B. N. Taylor and D. B. Newell, *Rev. Mod. Phys.*, 2008, **80**, 633–730.
35 J. F. Nye, *Physical Properties of Crystals*, Clarendon Press, Oxford, 1957.
36 Y. Noel and R. Dovesi, The evaluation of the elastic and piezoelectric tensors, CRYSTAL Tutorial Project, 2008, see http://www.crystal.unito.it/tutorials/.
37 F. D. Murnaghan, *Proc. Natl. Acad. Sci. U. S. A.*, 1944, **30**, 244–247.
38 O. L. Anderson, *J. Phys. Chem. Solids*, 1966, **27**, 547–565.
39 R. S. Berry, S. A. Rice and J. Ross, *Physical Chemistry*, Oxford University Press, New York, 2nd edn., 2000, ch. 24.
40 J. Zhang, S. Morlens, L. G. Hubert-Pfalzgraf and D. Luneau, *Eur. J. Inorg. Chem.*, 2005, 3928–3935.
41 N. Wiberg, *Holleman-Wiberg's Inorganic Chemistry*, Academic Press, San Diego, 2001, app. IV.
42 M. Nizam, Y. Bouteiller, B. Silvi, M. Causà and R. Dovesi, *J. Phys. C: Solid State Phys.*, 1988, **21**, 5351–5359.
43 M. W. Chase, Jr., *J. Phys. Chem. Ref. Data, Monogr. 9*, 1998, 1138ff.
44 L. Ehm, K. Knorr, F. Mädler, H. Voigtländer, E. Busetto, A. Cassetta, A. Lausi and B. Winkler, *J. Phys. Chem. Solids*, 2003, **64**, 919–925.
45 B. Paulus and K. Rosciszewski, *Chem. Phys. Lett.*, 2004, **394**, 96–100.
46 B. Paulus, *Phys. Rep.*, 2006, **428**, 1–52.
47 O. L. Anderson, *Equations of State of Solids for Geophysics and Ceramic Science*, Oxford University Press, New York, 1995.
48 D. P. Dandekar, J. J. Tsou and J. C. Ho, *Phys. Rev. B: Condens. Matter*, 1979, **20**, 3523–3525.
49 P. Schwerdtfeger, G. A. Heath, M. Dolg and M. A. Bennett, *J. Am. Chem. Soc.*, 1992, **114**, 7518–7527.
50 V. I. Bazhanov, *Zh. Strukt. Khim.*, 1991, **32**, 54–59 (*J. Struct. Chem.*, 1991, **32**, 44–48).